Mineralogical Magazine, June 2012, Vol. 76(3), pp. 551–566

A chemical and structural re-examination of fettelite samples from the type locality, Odenwald, southwest Germany

L. Bindi[1,2,*], R. T. Downs[3], P. G. Spry[4], W. W. Pinch[5] and S. Menchetti[1]

[1] Dipartimento di Scienze della Terra, Università degli Studi di Firenze, Via G. La Pira 4, I-50121 Firenze, Italy
[2] CNR – Istituto di Geoscienze e Georisorse, Sezione di Firenze, Via G. La Pira 4, I-50121 Firenze, Italy
[3] Department of Geosciences, University of Arizona, Tucson, Arizona 85721-0077, USA
[4] Department of Geological and Atmospheric Sciences, 253 Science I, Iowa State University, Ames, Iowa 50011-3212, USA
[5] 19 Stonebridge Lane, Pittsford, New York 14534, USA

[*Received 20 November 2011; Accepted 22 February 2012; Associate Editor: Allan Pring*]

ABSTRACT

The crystal structure and chemical composition of two samples of fettelite from the type locality, including a portion of the holotype material, was investigated to verify if a previously proposed revision of the chemical formula was applicable, and to study the role of cation substitution for Hg that would suggest new members of the fettelite family. The crystal structure of fettelite from the type locality was found to be equivalent to that reported previously for the Chilean occurrence, and consists of an alternation of two kinds of layers along *c*: layer *A* with general composition $[Ag_6As_2S_7]^{2-}$ and layer *B* with general composition $[Ag_{10}HgAs_2S_8]^{2+}$. In this structure, the Ag atoms occur in various coordination configurations, varying from quasi-linear to quasi-tetrahedral, the AsS_3 groups form pyramids as are typically observed in sulfosalts, and Hg links two sulfur atoms in a linear coordination. The refined compositions for the crystals in this study, $[Ag_6As_2S_7][Ag_{10}(Fe_{0.53}Hg_{0.47})As_2S_8]$ (R100124) and $[Ag_6As_2S_7][Ag_{10}(Hg_{0.79}Cu_{0.21})As_2S_8]$ (R110042), clearly indicate that new mineral species related to fettelite are likely to be found in nature.

Keywords: fettelite, Hg-sulfosalts, pearceite, polybasite, crystal structure, Glasberg quarry, Odenwald, Germany.

Introduction

Fettelite is a rare Hg-bearing sulfosalt that was first identified as a new mineral species by Wang and Paniagua (1996) during a study of silver minerals from the Glasberg quarry, Nieder-Beerbach, Odenwald, southwest Germany. Based on microprobe data, they reported an ideal chemical formula of $Ag_{24}HgAs_5S_{20}$. The crystal structure of fettelite was later solved and refined using intensity data collected from a twinned crystal from Chañarcillo, Copiapó Province, Chile, both at room temperature (Bindi *et al.*, 2009) and at high temperature (Bindi and Menchetti, 2011). The structural study at room temperature revealed that, in spite of strong hexagonal pseudosymmetry, the mineral is monoclinic (space group *C*2), intimately twinned with six twin domains, with a = 26.0388(10), b = 15.0651(8), c = 15.5361(8) Å, β = 90.48(1)º and V = 6094.2(5) Å^3. On the basis of the information gained from this characterization, Bindi *et al.* (2009) revised the crystal-chemical formula to

* E-mail: luca.bindi@unifi.it
DOI: 10.1180/minmag.2012.076.3.07

$[Ag_6As_2S_7][Ag_{10}HgAs_2S_8]$ (Z = 8) and discussed the relationships between the data obtained from the Chilean fettelite and those reported previously for the mineral from the type locality, concluding that a difference in chemical composition (especially the Ag/Hg ratio) could explain the dissimilarities observed in the unit-cell values. However, as Wang and Paniagua (1996) did not carry out a precise X-ray study on the type specimen of fettelite, questions remain as to whether or not there are different members of the fettelite family in nature. Recently, a new sample from the type locality (Glasberg quarry, Nieder-Beerbach, Odenwald, southwest Germany) was donated to the RRUFF collection (sample R100124) by one of the authors (WWP). This sample shows an anomalous enrichment in iron, which suggests that there may be a possible new Fe-rich endmember. Motivated by this observation and by the possibility that there could be different fettelite-like minerals, we requested a portion of the holotype specimen, which is housed in the mineral collection of the Institute of Mineralogy at the University of Heidelberg.

Here we present a structural and chemical characterization of two samples of fettelite from the type locality in order to verify whether the revised chemical formula proposed by Bindi *et al.* (2009) is applicable to the type fettelite sample, and to study the role of cation substitution for Hg, which might indicate new fettelite-like minerals.

Occurrence and physical and optical properties

The two samples studied here were not found *in situ*, but originate from the RRUFF Project collection (rruff.info/R100124, Fig. 1), and from a small portion (rruff.info/R110042, Fig. 2) of the holotype specimen, which is deposited in the Institute of Mineralogy at the University of Heidelberg. Both the fettelite samples come from the Glasberg quarry.

Fettelite from samples R100124 and R110042 is dark red to grey-black with a dark grey streak. It is opaque in transmitted light and has a metallic lustre. The crystals are brittle with perfect {001} cleavage and the fracture is uneven to subconchoidal. Micro-indentation measurements carried out with a VHN load of 20 g give a mean value of 122 kg mm^{-2} (range 111–131) and 143 kg mm^{-2} (range 131–150) for R100124 and R110042, respectively, corresponding to a Mohs hardness of about 3½.

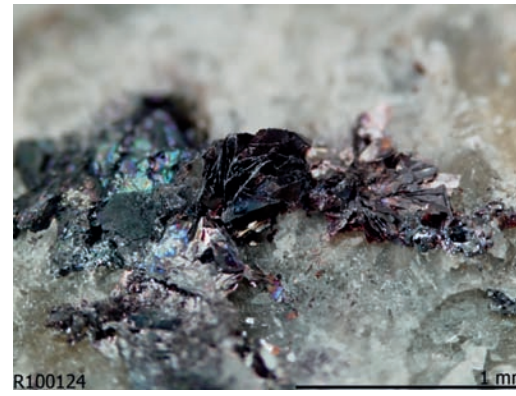

FIG. 1. One of the samples (R100124) containing dark red fettelite.

In plane-polarized incident light, fettelite from both samples is greyish white in colour, with moderate bireflectance (from white to brownish grey). Between crossed polars, it shows weak anisotropy, with relatively strong red internal reflections. Reflectance measurements were performed in air using a Zeiss MPM-200 microphotometer equipped with a MSP-20 system processor on a Zeiss Axioplan ore microscope. The filament temperature was approximately 3350 K. Four wavelengths (471.1, 548.3, 586.6, and 652.3 nm) produced by an interference filter were used for the measurements, which were obtained from the specimen and calibrated using an SiC standard in the same focus conditions. The diameter of the circular area

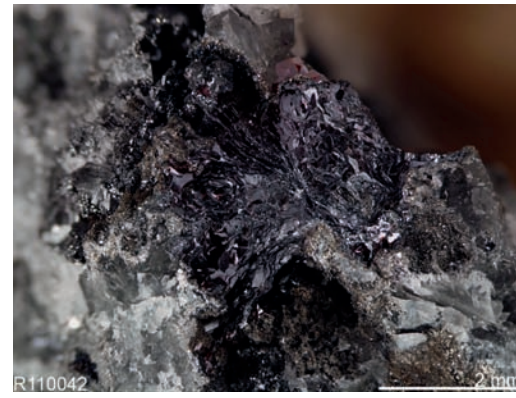

FIG. 2. Part of the holotype sample, R110042 containing dark red fettelite.

that was measured was 0.1 mm. Reflectance percentages for R_{min} and R_{max} are 28.2, 29.4 (471.1 nm), 25.0, 26.3 (548.3 nm), 22.9, 23.5 (586.6 nm), 20.9, 21.2 (652.3 nm), and 28.8, 29.9 (471.1 nm), 25.8, 27.0 (548.3 nm), 24.8, 25.6 (586.6 nm), 22.9, 23.7 (652.3 nm), for R100124 and R110042, respectively. Both of the fettelite samples from the type locality are slightly less reflective than fettelite from Chañarcillo (Bindi *et al.*, 2009).

Chemical composition

The chemical composition was determined using wavelength-dispersive spectrometry (WDS) by means of a JEOL JXA-8200 electron microprobe (sample R100124 and R110042) and a Cameca SX100 electron microprobe (sample R100124). Concentrations of major and minor elements were determined at an accelerating voltage of 15 kV and a beam current of 15 nA, with a 20 s counting time (spot size 1 μm). For the WDS analyses the following lines were used (for both the instruments): S$K\alpha$, Fe$K\alpha$, Cu$K\alpha$, As$L\alpha$, Ag$L\alpha$, Sb$L\beta$, Pb$M\alpha$ and Hg$L\alpha$. The standards employed were pure metals for Cu and Ag, galena for Pb, pyrite for Fe and S, cinnabar for Hg, synthetic Sb_2S_3 for Sb, and synthetic As_2S_3 for As. The fettelite fragments were homogeneous to within analytical error. The average chemical compositions and the atomic ratios on the basis of 36 atoms are reported in Table 1, together with the chemical data given by Wang and Paniagua (1996) for type fettelite, and those reported by Bindi *et al.* (2009) for Chilean fettelite. On the basis of 36 atoms (see the structure description), the formulae can be written as $Ag_{16.45}(Fe_{0.89}Hg_{0.37}Cu_{0.01})_{\Sigma=1.27}(As_{4.03}Sb_{0.04})_{\Sigma=4.07}S_{14.21}$ and $Ag_{16.08}(Hg_{0.71}Cu_{0.13}Fe_{0.01})_{\Sigma=0.85}As_{3.80}S_{15.27}$, for R100124 and R110042, respectively. It appears therefore that the chemical formulae are rather far from ideal [e.g. $\Sigma S = 15$ a.p.f.u., $\Sigma(As + Sb) = 4$ a.p.f.u., $Ag = 16$ a.p.f.u.]. It should be noted, however, that fettelite from the type locality is strongly sensitive to the electron beam, which makes it difficult to obtain precise and accurate

TABLE 1. Electron microprobe data (wt.% elements) and atomic ratios for fettelite.

	Type locality			Chañarcillo, Chile
	This study (R100124)	This study (R110042)	Wang and Paniagua (1996)	Bindi *et al.* (2009)
Ag	66.77	64.75	67.55	62.78
Cu	0.02	0.30	0.07	0.09
Pb	0.02	0.01	0.07	0.15
Tl	n.a.	n.a.	0.13	0.07
Fe	1.88	0.02	0.04	0.02
Hg	2.76	5.34	5.21	7.19
As	11.35	10.62	9.8	10.01
Sb	0.18	0.00	0.23	1.56
S	17.14	18.29	16.79	17.60
Total	100.12	99.33	99.89	99.47
Atomic ratio on the basis of 36 atoms				
Ag	16.45	16.08	17.19	15.92
Cu	0.01	0.13	0.03	0.04
Pb	0.00	0.00	0.01	0.02
Tl	–	–	0.02	0.01
Fe	0.89	0.01	0.02	0.01
Hg	0.37	0.71	0.71	0.98
As	4.03	3.80	3.59	3.65
Sb	0.04	0.00	0.05	0.35
S	14.21	15.27	14.38	15.02
Total	36.00	36.00	36.00	36.00

n.a.: not analysed.

microprobe data. Indeed, for most of the crystals, the electron beam caused Hg to vaporize from the sample and we observed a gradual reduction in the Hg content with time and corresponding damage to the sample surface. To minimize the beam damage, we reduced the beam current to 15 nA for the analyses listed in Table 1. It should be noted that Bindi *et al.* (2009) did not observe beam damage on the samples of fettelite from Chile. In that study, an accelerating voltage of 20 kV and a beam current of 40 nA were used. The reason for this difference is probably linked to the quality and the size of the crystals, which are larger and more homogeneous at the Chilean occurrence in comparison to the type locality (Figs 1 and 2; Wang and Paniagua, 1996).

X-ray crystallography

Two crystals were extracted from the polished microprobe sections produced from samples R100124 and R110042 and analysed using an Oxford Diffraction Xcalibur 3 diffractometer (Mo$K\alpha$ radiation, λ = 0.71073 Å) fitted with a Sapphire 2 CCD detector (see Table 2 for details). As fettelite is commonly twinned, a full diffraction sphere of diffraction data was collected from both crystals. Intensity integration and standard Lorentz-polarization corrections were done with the *CrysAlis RED* (Oxford Diffraction, 2006) software package. The *ABSPACK* program, which is part of *CrysAlis RED* (Oxford Diffraction, 2006), was used to make absorption corrections. Subsequent calculations were conducted using the *JANA2006* program suite (Petříček *et al.*, 2006).

The crystal structures were refined in space group *C*2 starting from the atom coordinates given by Bindi *et al.* (2009) for Chilean fettelite and taking into account the twin law that makes the twinned lattice appear to be hexagonal (i.e. twinning by metric merohedry; see Nespolo, 2004, and references therein). Refinement of the occupancy factors for all the Ag (Ag *vs*. Cu) atoms and for all the As (As *vs*. Sb) atoms for R100124 and R110042 produced site-scattering values consistent with pure Ag and As, respectively, but the Hg positions were partially occupied by a lighter element. In view of the WDS data, we chose to refine Hg *vs*. Fe for R100124, and Hg *vs*. Cu for R110042 (Table 3). At this stage, the residual values converged from R = 0.065 to R = 0.058 for R100124, and from R = 0.072 to R = 0.069 for R110042 [2σ(I) level], including all the collected reflections in the refinements. Based on these refinements, analyses of the difference Fourier synthesis maps suggested an additional twofold twin axis perpendicular to the previously determined threefold axis, leading to a second-degree twin. The introduction of only three new parameters (the new twin volume ratios) lowered the R values to 0.045 (R100124) and 0.057 (R110042), although the new domains were rather small in size (Table 2). At the last stage, using anisotropic displacement parameters for all atoms and no constraints, the residual values settled at R = 0.031 for 8136 independent observed reflections [2σ(I) level] and 659 parameters and at R = 0.034 for all 16,981 independent reflections for R100124, and at R = 0.043 for 7445 independent observed reflections [2σ(I) level] and 659 parameters and at R = 0.049 for all 17,368 independent reflections for R110042.

Table 2 contains further details of the refinement. Fractional atom coordinates and isotropic displacement parameters are given in Table 3. Bond distances are listed in Table 4. Anisotropic displacement parameters and the structure factors for R100124 and R110042 (in Supplementary Tables 5, 6 and 7, respectively) have been deposited with the Principal Editors of *Mineralogical Magazine* and are available at http://www.minersoc.org/pages/e_journals/dep_mat.html.

Description of the structure and discussion

The crystal structure of fettelite from the type locality is equivalent to that previously reported by Bindi *et al.* (2009) from the Chilean occurrence. Briefly, the structure can be described as the alternation of two kinds of layers along *c* (Fig. 3): layer *A* with a general composition $[Ag_6As_2S_7]^{2-}$ and layer *B* with a general composition $[Ag_{10}HgAs_2S_8]^{2+}$. In this structure, the Ag atoms occur in various coordination configurations, varying from quasi-linear to quasi-tetrahedral, the AsS_3 groups form pyramids as are typically observed in sulfosalts, and the Hg atom links two sulfur atoms in a linear coordination (Table 4). The bond distances observed are consistent with those found for Chilean fettelite (Bindi *et al.*, 2009) and for other Ag-bearing sulfosalts (e.g. proustite, pyrargyrite, pearceite, polybasite and stephanite). Fettelite has a module layer with a composition $[Ag_6As_2S_7]^{2-}$ (i.e. the *A* layer), which is identical to that in

TABLE 2. Details pertaining to the single-crystal X-ray data collections and structure refinements of the two fettelite crystals.

	Sample R100124	Sample R110042
Crystal data		
Formula	$[Ag_6As_2S_7][Ag_{10}(Fe_{0.53}Hg_{0.47})As_2S_8]$	$[Ag_6As_2S_7][Ag_{10}(Hg_{0.79}Cu_{0.21})As_2S_8]$
Crystal size (mm)	$0.078 \times 0.072 \times 0.011$	$0.058 \times 0.069 \times 0.010$
Form	platy	platy
Colour	dark red	dark red
Crystal system	monoclinic	monoclinic
Space group	*C*2	*C*2
a (Å)	26.011(2)	26.030(2)
b (Å)	15.048(1)	15.059(1)
c (Å)	15.513(1)	15.524(1)
β (°)	90.40(1)	90.45(1)
V (Å^3)	6071.9(7)	6085.0(7)
Z	8	8
Instrumental collection		
Instrument	Oxford Diffraction Excalibur 3	Oxford Diffraction Excalibur 3
Radiation type	Mo*K*α (λ = 0.71073)	Mo*K*α (λ = 0.71073)
Temperature (K)	298(3)	298(3)
Detector to sample distance (cm)	5	5
Number of frames	3127	3110
Measuring time (s)	185	200
Maximum 2θ (°)	69.68	69.58
Absorption correction	multi-scan (*ABSPACK*; Oxford Diffraction 2006)	multi-scan (*ABSPACK*; Oxford Diffraction 2006)
Collected reflections	70,024	69,857
Unique reflections	16,981	17,368
Reflections with $F_o > 4\ \sigma\ (F_o)$	8136	7445
R_{int}	0.0423	0.0389
R_σ	0.0398	0.0362
Range *h*, *k*, *l*	$-40 \leqslant h \leqslant 41$, $-23 \leqslant k \leqslant 23$, $-24 \leqslant l \leqslant 24$	$-40 \leqslant h \leqslant 41$, $-23 \leqslant k \leqslant 23$, $-24 \leqslant l \leqslant 24$
Refinement		
Refinement	Full-matrix least squares on F^2	Full-matrix least squares on F^2
Twin matrices	$\begin{bmatrix}1&0&0\\0&1&0\\0&0&1\end{bmatrix}, \begin{bmatrix}-0.5&-0.5&0\\1.5&-0.5&0\\0&0&1\end{bmatrix}, \begin{bmatrix}-0.5&0.5&0\\-1.5&-0.5&0\\0&0&1\end{bmatrix}$ $\begin{bmatrix}-1&0&0\\0&-1&0\\0&0&-1\end{bmatrix}, \begin{bmatrix}0.5&0.5&0\\-1.5&0.5&0\\0&0&1\end{bmatrix}, \begin{bmatrix}0.5&-0.5&0\\1.5&0.5&0\\0&0&1\end{bmatrix}$	$\begin{bmatrix}1&0&0\\0&1&0\\0&0&1\end{bmatrix}, \begin{bmatrix}-0.5&-0.5&0\\1.5&-0.5&0\\0&0&1\end{bmatrix}, \begin{bmatrix}-0.5&0.5&0\\-1.5&-0.5&0\\0&0&1\end{bmatrix}$ $\begin{bmatrix}-1&0&0\\0&-1&0\\0&0&-1\end{bmatrix}, \begin{bmatrix}0.5&0.5&0\\-1.5&0.5&0\\0&0&1\end{bmatrix}, \begin{bmatrix}0.5&-0.5&0\\1.5&0.5&0\\0&0&1\end{bmatrix}$
Twin volume fractions	0.3965(9), 0.3875(7), 0.1002(8) 0.0425(4), 0.0305(3), 0.0428(4)	0.4125(7), 0.3798(7), 0.0987(8) 0.0385(4), 0.0284(3), 0.0421(4)
Final *R* [$I > 2\ \sigma\ (I)$]	0.0314	0.0430
Final *R* (all data)	0.0341	0.0489
Number of least squares parameters	659	659
$\Delta\rho_{max}$ (e Å^{-3})	1.13	3.96
$\Delta\rho_{min}$ (e Å^{-3})	−1.40	−1.23

Note that $R = \Sigma||F_o|-|F_c|| / \Sigma|F_o|$; $wR^2 = [\ \Sigma\ w\ (|F_o|^2 - |F_c|^2)^2 / \Sigma\ w\ (|F_o|^4)]^{1/2}$.

TABLE 3. Wyckoff positions, site occupancy factors, fractional atom coordinates, and equivalent isotropic displacement parameters (Å^2) for the selected fettelite crystals.

Atom	Wyckoff	S. O. F.	*x*/*a*	*y*/*b*	*z*/*c*	U_{iso}
R100124						
Fe1	4*c*	0.546(2)	0.12290(1)	0.10428(2)	0.50143(2)	0.0175(1)
Hg1	4*c*	0.454	0.12290(1)	0.10428(2)	0.50143(2)	0.0175(1)
Fe2	4*c*	0.506(2)	0.13030(1)	0.61018(2)	0.50011(2)	0.0173(1)
Hg2	4*c*	0.494	0.13030(1)	0.61018(2)	0.50011(2)	0.0173(1)
Ag1	4*c*	1.00	0.28021(2)	0.83512(3)	0.91440(3)	0.0259(1)
Ag2	4*c*	1.00	0.07835(2)	0.46559(3)	0.08702(3)	0.0247(1)
Ag3	4*c*	1.00	0.04773(2)	0.61816(3)	−0.09586(2)	0.02018(9)
Ag4	4*c*	1.00	−0.02857(2)	0.38326(2)	0.08976(2)	0.01871(8)
Ag5	4*c*	1.00	−0.03304(2)	−0.11835(3)	0.08981(2)	0.01957(8)
Ag6	4*c*	1.00	0.07675(2)	−0.02592(3)	0.08682(3)	0.02065(9)
Ag7	4*c*	1.00	0.04689(2)	0.11624(3)	0.90526(2)	0.01833(8)
Ag8	4*c*	1.00	0.16703(2)	0.24525(2)	0.91108(2)	0.01903(8)
Ag9	4*c*	1.00	0.20499(2)	0.09411(3)	0.09844(3)	0.0254(1)
Ag10	4*c*	1.00	0.28137(2)	0.32277(3)	0.91184(3)	0.02240(9)
Ag11	4*c*	1.00	0.17836(2)	0.74447(2)	0.91295(2)	0.01897(8)
Ag12	4*c*	1.00	0.20062(2)	0.60923(3)	0.09394(2)	0.02076(8)
Ag13	4*c*	1.00	0.12902(2)	−0.12902(3)	0.71083(3)	0.02133(8)
Ag14	4*c*	1.00	0.11669(2)	0.62581(3)	0.30174(3)	0.02276(9)
Ag15	4*c*	1.00	0.01731(2)	0.72843(2)	0.30764(2)	0.01605(8)
Ag16	4*c*	1.00	0.01448(2)	0.22697(2)	0.29593(2)	0.01684(7)
Ag17	4*c*	1.00	0.13161(2)	0.37402(3)	0.70735(2)	0.02002(8)
Ag18	4*c*	1.00	0.23521(2)	0.48299(3)	0.69742(2)	0.01990(9)
Ag19	4*c*	1.00	0.11995(2)	0.12830(3)	0.30838(3)	0.02386(9)
Ag20	2*b*	1.00	0	0.75526(4)	½	0.0189(1)
Ag21	4*c*	1.00	0.13656(2)	0.07341(2)	0.69020(2)	0.01554(7)
Ag22	4*c*	1.00	0.18300(2)	0.29319(2)	0.50033(2)	0.01686(8)
Ag23	4*c*	1.00	0.13753(2)	0.57402(3)	0.69499(2)	0.01912(8)
Ag24	4*c*	1.00	0.11434(2)	0.32675(3)	0.29817(3)	0.02107(8)
Ag25	4*c*	1.00	0.17829(2)	0.80086(3)	0.49719(2)	0.02178(9)
Ag26	4*c*	1.00	0.23462(2)	−0.01597(2)	0.69520(2)	0.01659(8)
Ag27	4*c*	1.00	0.06952(2)	−0.08556(3)	0.50162(2)	0.01937(8)
Ag28	4*c*	1.00	0.11663(2)	0.83269(3)	0.29454(3)	0.02098(9)
Ag29	4*c*	1.00	0.24802(1)	0.13711(3)	0.50137(1)	0.01682(9)
Ag30	2*b*	1.00	0	0.28369(4)	½	0.0191(1)
Ag31	4*c*	1.00	0.24856(1)	0.45515(3)	0.50208(1)	0.01653(9)
Ag32	2*b*	1.00	0	0.09672(4)	½	0.0240(1)
Ag33	4*c*	1.00	0.07230(2)	0.41941(3)	0.50040(2)	0.02052(8)
Ag34	2*b*	1.00	0	0.56031(4)	½	0.01567(9)
As1	4*c*	1.00	0.08444(3)	0.22513(4)	0.07232(4)	0.0220(1)
As2	4*c*	1.00	0.08084(3)	0.72355(4)	0.07285(3)	0.0203(1)
As3	4*c*	1.00	0.16626(3)	0.48536(4)	0.92769(3)	0.0184(1)
As4	4*c*	1.00	0.16989(3)	−0.01196(4)	0.92668(4)	0.0216(1)
As5	4*c*	1.00	0.24901(2)	0.73297(3)	0.28512(3)	0.0170(1)
As6	4*c*	1.00	0.00013(2)	0.47190(4)	0.28488(3)	0.0180(1)
As7	4*c*	1.00	0.00114(2)	−0.02438(3)	0.71439(3)	0.0142(1)
As8	4*c*	1.00	0.25028(2)	0.23298(3)	0.28479(3)	0.0150(1)
S1	4*c*	1.00	0.00661(6)	0.74554(9)	0.15107(8)	0.0223(3)
S2	4*c*	1.00	0.11788(6)	0.11159(10)	0.15381(8)	0.0249(3)
S3	4*c*	1.00	0.24226(6)	0.46568(8)	0.85759(7)	0.0178(2)
S4	4*c*	1.00	0.13515(5)	0.60325(7)	0.85525(7)	0.0140(2)
S5	4*c*	1.00	0.01035(5)	0.24233(7)	0.13887(7)	0.0168(2)
S6	4*c*	1.00	0.12487(6)	−0.11805(8)	0.87426(8)	0.0203(3)

TABLE 3 (*contd.*)

Atom	Wyckoff	S. O. F.	*x*/*a*	*y*/*b*	*z*/*c*	U_{iso}
S7	4*c*	1.00	0.12064(6)	0.37808(8)	0.86105(8)	0.0198(3)
S8	4*c*	1.00	0.12282(5)	0.83964(7)	0.12975(7)	0.0143(2)
S9	4*c*	1.00	0.11306(6)	0.61056(9)	0.14685(7)	0.0191(2)
S10	4*c*	1.00	0.12580(6)	0.33539(10)	0.13245(8)	0.0220(3)
S11	4*c*	1.00	0.24145(6)	−0.02660(8)	0.85481(7)	0.0167(2)
S12	4*c*	1.00	0.25443(5)	0.69873(9)	−0.00351(5)	0.0190(3)
S13	4*c*	1.00	0.13136(5)	0.09774(7)	0.85122(6)	0.0129(2)
S14	2*a*	1.00	0	0.51168(9)	0	0.0130(3)
S15	2*a*	1.00	0	0.01297(11)	0	0.0200(3)
S16	4*c*	1.00	0.21319(6)	0.84667(8)	0.35884(7)	0.0160(2)
S17	4*c*	1.00	0.07400(5)	−0.02650(7)	0.35289(7)	0.0158(2)
S18	4*c*	1.00	0.08550(5)	0.73689(7)	0.46472(6)	0.0156(2)
S19	4*c*	1.00	0.08326(5)	0.22844(7)	0.44726(7)	0.0172(2)
S20	4*c*	1.00	0.16669(4)	−0.02623(6)	0.53039(6)	0.0131(2)
S21	4*c*	1.00	0.21299(6)	0.61444(7)	0.35125(7)	0.0147(2)
S22	4*c*	1.00	0.07369(5)	0.47227(7)	0.35161(6)	0.0116(2)
S23	4*c*	1.00	0.04260(6)	−0.13486(8)	0.65087(8)	0.0180(2)
S24	4*c*	1.00	−0.03842(6)	0.36196(8)	0.34823(7)	0.0147(2)
S25	4*c*	1.00	−0.03742(6)	0.58788(7)	0.35383(7)	0.0155(2)
S26	4*c*	1.00	0.17414(5)	0.23817(7)	0.64448(7)	0.0145(2)
S27	4*c*	1.00	0.21099(5)	0.34744(6)	0.35752(6)	0.0106(2)
S28	4*c*	1.00	0.28549(6)	0.61957(8)	0.65009(7)	0.0159(2)
S29	4*c*	1.00	−0.03374(5)	0.08965(6)	0.36107(6)	0.0110(2)
S30	4*c*	1.00	0.16878(6)	0.72989(8)	0.64438(7)	0.0178(2)
S31	4*c*	1.00	0.16113(4)	0.47849(5)	0.55879(5)	0.0104(2)
R110042						
Hg1	4*c*	0.811(4)	0.12317(5)	0.10741(6)	0.50142(7)	0.0259(3)
Cu1	4*c*	0.189	0.12317(5)	0.10741(6)	0.50142(7)	0.0259(3)
Hg2	4*c*	0.762(4)	0.13044(4)	0.61371(6)	0.50032(7)	0.0245(3)
Cu2	4*c*	0.238	0.13044(4)	0.61371(6)	0.50032(7)	0.0245(3)
Ag1	4*c*	1.00	0.27942(7)	0.83547(9)	0.9149(1)	0.0303(4)
Ag2	4*c*	1.00	0.07787(7)	0.46518(8)	0.0867(1)	0.0231(4)
Ag3	4*c*	1.00	0.04799(6)	0.61918(9)	−0.09576(9)	0.0207(3)
Ag4	4*c*	1.00	−0.02886(7)	0.38295(9)	0.0896(1)	0.0276(4)
Ag5	4*c*	1.00	−0.03282(7)	−0.11871(9)	0.0902(1)	0.0269(4)
Ag6	4*c*	1.00	0.07739(7)	−0.02527(8)	0.0867(1)	0.0240(4)
Ag7	4*c*	1.00	0.04706(7)	0.1177(1)	0.9050(1)	0.0304(4)
Ag8	4*c*	1.00	0.16718(7)	0.24399(8)	0.9108(1)	0.0240(4)
Ag9	4*c*	1.00	0.20512(7)	0.09588(9)	0.0978(1)	0.0301(4)
Ag10	4*c*	1.00	0.28159(6)	0.32376(8)	0.9115(1)	0.0234(4)
Ag11	4*c*	1.00	0.17838(7)	0.74481(9)	0.9122(1)	0.0287(4)
Ag12	4*c*	1.00	0.20066(7)	0.6100(1)	0.0936(1)	0.0330(4)
Ag13	4*c*	1.00	0.12931(6)	−0.12908(8)	0.7113(1)	0.0227(3)
Ag14	4*c*	1.00	0.11725(6)	0.62574(9)	0.3026(1)	0.0288(4)
Ag15	4*c*	1.00	0.01748(7)	0.72701(9)	0.3082(1)	0.0262(4)
Ag16	4*c*	1.00	0.01481(7)	0.2264(1)	0.2965(1)	0.0304(4)
Ag17	4*c*	1.00	0.13132(6)	0.37339(8)	0.70689(9)	0.0196(3)
Ag18	4*c*	1.00	0.23574(7)	0.48206(8)	0.6980(1)	0.0248(4)
Ag19	4*c*	1.00	0.12004(6)	0.12922(9)	0.3083(1)	0.0264(4)
Ag20	2*b*	1.00	0	0.7316(1)	½	0.0302(5)
Ag21	4*c*	1.00	0.13640(6)	0.07349(9)	0.6898(1)	0.0239(3)
Ag22	4*c*	1.00	0.18294(6)	0.29352(9)	0.5007(1)	0.0268(4)
Ag23	4*c*	1.00	0.13781(7)	0.57552(9)	0.6945(1)	0.0282(4)

TABLE 3 (*contd.*)

Atom	Wyckoff	S. O. F.	*x*/*a*	*y*/*b*	*z*/*c*	U_{iso}
Ag24	4*c*	1.00	0.11447(6)	0.32572(8)	0.29886(9)	0.0221(3)
Ag25	4*c*	1.00	0.17866(6)	0.80057(9)	0.4976(1)	0.0258(4)
Ag26	4*c*	1.00	0.23458(7)	−0.01717(8)	0.6953(1)	0.0269(4)
Ag27	4*c*	1.00	0.06951(6)	−0.08579(8)	0.50236(9)	0.0211(3)
Ag28	4*c*	1.00	0.11660(7)	0.83255(9)	0.2937(1)	0.0283(4)
Ag29	4*c*	1.00	0.24810(6)	0.13996(7)	0.50085(9)	0.0220(3)
Ag30	2*b*	1.00	0	0.2874(1)	½	0.0230(5)
Ag31	4*c*	1.00	0.24918(7)	0.44863(8)	0.5017(1)	0.0234(3)
Ag32	2*b*	1.00	0	0.0945(1)	½	0.0262(5)
Ag33	4*c*	1.00	0.07276(6)	0.41872(9)	0.50135(9)	0.0222(4)
Ag34	2*b*	1.00	0	0.5762(1)	½	0.0217(5)
As1	4*c*	1.00	0.08490(9)	0.2250(1)	0.07298(13)	0.0233(5)
As2	4*c*	1.00	0.0806(1)	0.7248(1)	0.0741(1)	0.0257(6)
As3	4*c*	1.00	0.16697(9)	0.4856(1)	0.9289(1)	0.0211(6)
As4	4*c*	1.00	0.16915(9)	−0.0125(1)	0.9266(1)	0.0194(5)
As5	4*c*	1.00	0.24888(9)	0.7325(1)	0.2850(1)	0.0207(5)
As6	4*c*	1.00	0.00058(9)	0.4716(1)	0.2860(1)	0.0208(5)
As7	4*c*	1.00	0.00114(9)	−0.0244(1)	0.7149(1)	0.0209(5)
As8	4*c*	1.00	0.25080(9)	0.2328(1)	0.2849(1)	0.0200(5)
S1	4*c*	1.00	0.0061(2)	0.7417(3)	0.1519(4)	0.033(1)
S2	4*c*	1.00	0.1173(3)	0.1103(3)	0.1532(4)	0.039(2)
S3	4*c*	1.00	0.2440(3)	0.4662(3)	0.8581(4)	0.039(2)
S4	4*c*	1.00	0.1353(2)	0.6030(3)	0.8549(4)	0.030(1)
S5	4*c*	1.00	0.0105(3)	0.2421(4)	0.1396(4)	0.042(2)
S6	4*c*	1.00	0.1261(2)	−0.1170(3)	0.8736(3)	0.031(1)
S7	4*c*	1.00	0.1212(2)	0.3769(3)	0.8620(4)	0.029(1)
S8	4*c*	1.00	0.1228(2)	0.8401(3)	0.1300(4)	0.035(2)
S9	4*c*	1.00	0.1128(2)	0.6095(3)	0.1467(4)	0.034(1)
S10	4*c*	1.00	0.1258(3)	0.3348(3)	0.1339(4)	0.037(2)
S11	4*c*	1.00	0.2417(3)	−0.0276(3)	0.8567(4)	0.042(2)
S12	4*c*	1.00	0.2542(2)	0.7008(3)	−0.0032(3)	0.034(1)
S13	4*c*	1.00	0.1325(3)	0.0953(3)	0.8512(4)	0.037(2)
S14	2*a*	1.00	0	0.5141(5)	0	0.040(2)
S15	2*a*	1.00	0	0.0140(4)	0	0.032(2)
S16	4*c*	1.00	0.2133(3)	0.8494(3)	0.3597(4)	0.038(2)
S17	4*c*	1.00	0.0755(3)	−0.0261(3)	0.3536(4)	0.037(2)
S18	4*c*	1.00	0.0857(2)	0.7403(3)	0.4531(4)	0.032(1)
S19	4*c*	1.00	0.0828(3)	0.2305(3)	0.4414(4)	0.038(2)
S20	4*c*	1.00	0.1668(3)	−0.0242(3)	0.5465(4)	0.034(2)
S21	4*c*	1.00	0.2126(2)	0.6145(3)	0.3510(4)	0.036(1)
S22	4*c*	1.00	0.0742(3)	0.4732(3)	0.3511(4)	0.037(2)
S23	4*c*	1.00	0.0431(3)	−0.1346(3)	0.6504(4)	0.034(1)
S24	4*c*	1.00	−0.0376(3)	0.3610(3)	0.3509(4)	0.034(2)
S25	4*c*	1.00	−0.0358(2)	0.5870(3)	0.3551(4)	0.031(1)
S26	4*c*	1.00	0.1733(2)	0.2390(3)	0.6447(4)	0.033(2)
S27	4*c*	1.00	0.2113(3)	0.3491(3)	0.3564(4)	0.033(2)
S28	4*c*	1.00	0.2857(2)	0.6165(4)	0.6493(4)	0.036(1)
S29	4*c*	1.00	−0.0336(2)	0.0893(3)	0.3612(4)	0.033(1)
S30	4*c*	1.00	0.1692(3)	0.7296(3)	0.6442(4)	0.038(2)
S31	4*c*	1.00	0.1605(3)	0.4818(3)	0.5593(4)	0.033(2)

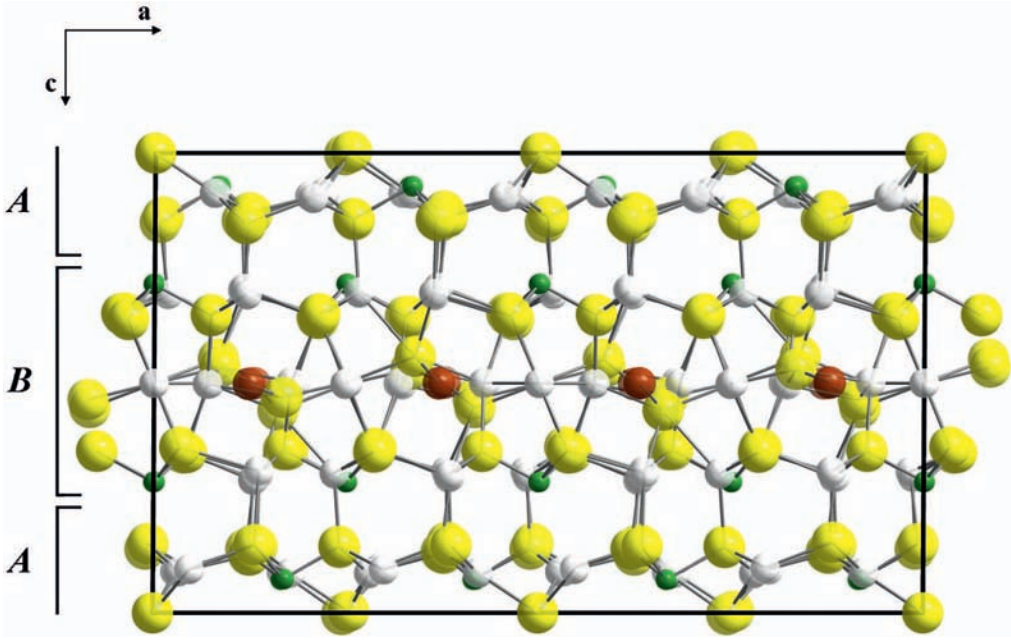

FIG. 3. A projection of the fettelite structure along the monoclinic *b* axis, emphasizing the succession of the $[Ag_6As_2S_7]^{2-}$ *A* and $[Ag_{10}HgAs_2S_8]^{2+}$ *B* module layers. White, green, brown and yellow circles indicate Ag, As, Hg and S atoms, respectively. The unit cell is outlined.

pearceite–polybasite (Bindi *et al.*, 2007*a* and references therein).

The crystal-structure refinement of fettelite R100124 showed that the Hg structural positions in the *B* module layer are largely occupied by iron (Table 3). Iron is the dominant cation on the basis of both X-ray structural formula (Tables 2, 3) and the electron microprobe data (Table 1). The Fe ↔ Hg substitution is also indicated if the mean bond distances of the two Hg positions are considered (Table 4). The <Hg–S> distances are shorter in R100124 than those found for sites that are fully occupied by Hg (Bindi *et al.*, 2009). Nevertheless, given the discrepancies between the formulae obtained using the two techniques, i.e. $Ag_{16.45}(Fe_{0.89}Hg_{0.37}Cu_{0.01})_{\Sigma=1.27}(As_{4.03}Sb_{0.04})_{\Sigma=4.07}S_{14.21}$ (WDS) and $Ag_{16}(Fe_{0.53}Hg_{0.47})_{\Sigma=1.00}As_4S_{15}$ (single-crystal XRD), we prefer not to propose R100124 as a new mineral to the IMA-CNMNC at this time. Unfortunately, the lack of published data for a structure having a linearly coordinated structural site fully occupied by Fe also precludes the possibility of making crystal-chemical considerations for the Hg–Fe join of fettelite (the dotted line in Fig. 4).

Some observations can be made on type fettelite (R110042). The structure refinement for this crystal shows that the Hg positions contain a significant amount of Cu (Table 3). The resulting mean bond distances for these positions, linearly coordinated by sulfur atoms, are 2.355 and 2.335 Å, respectively (Table 4). Taking into account all the Hg–S distances in the structure of Chilean fettelite (Bindi *et al.*, 2009) and those observed for members of the pearceite–polybasite group (Bindi *et al.*, 2006, 2007*b*, 2007*c*; Evain *et al.*, 2006), which have Cu in a similar crystal-chemical environment (linearly coordinated by two sulfur atoms), the following equation is obtained:

$$\text{<Hg–S>}\ (\text{Å}) = 2.159(2) + 0.238(4)\text{Hg}\ (\text{a.p.f.u.})$$

This is shown as a dashed line in Fig. 4, and it indicates that if a mean bond distance that is of less than 2.276 Å is measured (calculated with Hg = 0.49 a.p.f.u.) for the Hg positions, and Cu ↔ Hg is the only cation substitution occurring at the Hg sites, the mineral could be a Cu-dominant analogue of fettelite. It is obvious that a Cu ↔ Hg substitution at the Hg sites would not be the

TABLE 4. The principal interatomic distances (Å) and their standard deviations (in parentheses) for the selected fettelite crystals.

R100124					
$[Ag_6As_2S_7]^{2-}$ ***A layer***					
As1–S10	2.183(2)	As2–S9	2.213(2)		
–S5	2.208(1)	–S8	2.238(2)		
–S2	2.293(2)	–S1	2.311(1)		
<As1–S>	**2.228**	**<As2–S>**	**2.254**		
As3–S4	2.248(1)	As4–S6	2.137(2)		
–S7	2.251(2)	–S11	2.188(1)		
–S3	2.282(1)	–S13	2.255(1)		
<As1–S>	**2.260**	**<As1–S>**	**2.193**		
Ag1–S11	2.488(1)	Ag2–S10	2.418(2)	Ag3–S4	2.413(1)
–S12	2.509(1)	–S14	2.5334(7)	–S14	2.5191(9)
–S10	2.555(2)	–S9	2.535(2)	–S1	2.528(1)
<Ag1–S>	**2.517**	**<Ag2–S>**	**2.495**	**<Ag3–S>**	**2.487**
Ag4–S5	2.468(1)	Ag5–S6	2.457(2)	Ag6–S8	2.442(1)
–S14	2.498(1)	–S1	2.480(2)	–S15	2.4707(7)
–S7	2.520(1)	–S15	2.569(1)	–S2	2.548(2)
<Ag4–S>	**2.495**	**<Ag5–S>**	**2.502**	**<Ag6–S>**	**2.487**
Ag7–S13	2.374(1)	Ag8–S7	2.458(1)	Ag9–S12	2.405(1)
–S15	2.467(1)	–S13	2.577(1)	–S2	2.443(2)
–S5	2.504(1)	–S12	2.584(1)	–S3	2.464(1)
<Ag7–S>	**2.448**	**<Ag8–S>**	**2.540**	**<Ag9–S>**	**2.437**
Ag10–S3	2.521(1)	Ag11–S12	2.456(1)	Ag12–S9	2.426(1)
–S12	2.528(1)	–S6	2.562(1)	–S12	2.467(1)
–S8	2.591(1)	–S4	2.563(1)	–S11	2.658(1)
<Ag10–S>	**2.547**	**<Ag11–S>**	**2.527**	**<Ag12–S>**	**2.517**
$[Ag_{10}(Fe,Hg)As_2S_8]^{2+}$ ***B layer***					
As5–S16	2.262(1)	As6–S22	2.169(1)		
–S21	2.264(1)	–S24	2.173(1)		
–S26	2.273(2)	–S25	2.271(1)		
<As5–S>	**2.266**	**<As6–S>**	**2.204**		
As7–S17	2.210(2)	As8–S28	2.194(1)		
–S23	2.216(1)	–S27	2.302(1)		
–S29	2.247(1)	–S30	2.369(2)		
<As7–S>	**2.224**	**<As8–S>**	**2.288**		
Fe1/Hg1–S19	2.291(1)	Fe2/Hg2–S18	2.299(1)		
–S20	2.313(1)	–S31	2.3213(9)		
<Fe1/Hg1–S>	**2.302**	**<Fe2/Hg2–S>**	**2.310**		
Ag20–S18	2.311(1)	Ag29–S28	2.514(1)	Ag32–S29	2.324(1)
–S18	2.311(1)	–S21	2.518(1)	–S29	2.324(1)
<Ag20–S>	**2.311**	**<Ag29–S>**	**2.516**	**<Ag32–S>**	**2.324**
Ag34–S25	2.496(1)	Ag33–S22	2.442(1)	Ag13–S23	2.428(2)
–S25	2.496(1)	–S31	2.631(1)	–S6	2.544(1)
<Ag34–S>	**2.496**	–S24	2.658(1)	–S30	2.580(1)
		<Ag33–S>	**2.567**	**<Ag13–S>**	**2.517**
Ag14–S9	2.415(1)	Ag15–S1	2.456(1)	Ag21–S13	2.529(1)
–S21	2.620(2)	–S25	2.651(1)	–S26	2.760(1)
–S22	2.683(1)	–S23	2.663(1)	–S29	2.796(2)
<Ag14–S>	**2.573**	**<Ag15–S>**	**2.590**	**<Ag21–S>**	**2.695**

Ag22–S26	2.397(1)	Ag26–S11	2.486(1)	Ag28–S17	2.560(1)
–S27	2.4753(9)	–S21	2.498(1)	–S8	2.565(1)
–S19	2.886(2)	–S27	2.629(1)	–S16	2.704(2)
<Ag22–S>	**2.586**	**<Ag26–S>**	**2.538**	**<Ag28–S>**	**2.610**
Ag16 –S5	2.449(1)	Ag17–S7	2.404(1)	Ag18–S3	2.504(1)
–S24	2.587(1)	–S26	2.524(1)	–S28	2.547(1)
–S29	2.623(1)	–S24	2.573(2)	–S16	2.605(1)
–S19	2.942(2)	–S31	2.8978(9)	–S31	2.878(1)
<Ag16–S>	**2.650**	**<Ag17–S>**	**2.600**	**<Ag18–S>**	**2.634**
Ag19–S2	2.411(1)	Ag23–S4	2.526(1)	Ag24–S22	2.571(1)
–S28	2.542(2)	–S30	2.605(1)	–S10	2.593(1)
–S17	2.710(1)	–S31	2.6317(8)	–S27	2.689(2)
–S19	2.802(1)	–S25	2.715(2)	–S19	2.867(1)
<Ag19–S>	**2.616**	**<Ag23–S>**	**2.619**	**<Ag24–S>**	**2.680**
Ag25–S16	2.436(1)	Ag27–S17	2.476(1)	Ag30–S19	2.465(1)
–S30	2.534(1)	–S23	2.535(1)	–S19	2.465(1)
–S18	2.644(1)	–S20	2.714(1)	–S24	2.810(1)
–S20	2.670(1)	–S18	2.764(1)	–S24	2.810(1)
<Ag25–S>	**2.571**	**<Ag27–S>**	**2.622**	**<Ag30–S>**	**2.638**
Ag31–S20	2.282(1)				
–S31	2.469(1)				
–S16	2.878(1)				
–S27	2.929(1)				
<Ag31–S>	**2.640**				

R110042

$[Ag_6As_2S_7]^{2-}$ ***A layer***

As1–S10	2.179(6)	As2–S9	2.231(6)		
–S5	2.218(6)	–S8	2.228(6)		
–S2	2.286(6)	–S1	2.305(6)		
<As1–S>	**2.228**	**<As2–S>**	**2.255**		
As3–S4	2.260(6)	As4–S6	2.095(6)		
–S7	2.271(6)	–S11	2.196(6)		
–S3	2.312(6)	–S13	2.213(6)		
<As1–S>	**2.281**	**<As1–S>**	**2.168**		
Ag1–S11	2.453(7)	Ag2–S10	2.436(6)	Ag3–S4	2.417(5)
–S12	2.485(5)	–S14	2.533(3)	–S14	2.511(5)
–S10	2.586(6)	–S9	2.531(6)	–S1	2.475(6)
<Ag1–S>	**2.508**	**<Ag2–S>**	**2.500**	**<Ag3–S>**	**2.468**
Ag4–S5	2.477(6)	Ag5–S6	2.498(6)	Ag6–S8	2.439(6)
–S14	2.533(6)	–S1	2.520(5)	–S15	2.486(3)
–S7	2.525(6)	–S15	2.589(5)	–S2	2.508(6)
<Ag4–S>	**2.512**	**<Ag5–S>**	**2.536**	**<Ag6–S>**	**2.478**
Ag7–S13	2.407(6)	Ag8–S7	2.449(5)	Ag9–S12	2.407(5)
–S15	2.478(5)	–S13	2.583(6)	–S2	2.459(6)
–S5	2.493(7)	–S12	2.574(6)	–S3	2.453(6)
<Ag7–S>	**2.459**	**<Ag8–S>**	**2.535**	**<Ag9–S>**	**2.440**
Ag10–S3	2.497(6)	Ag11–S12	2.453(6)	Ag12–S9	2.438(6)
–S12	2.520(5)	–S6	2.555(5)	–S12	2.471(5)
–S8	2.586(6)	–S4	2.567(6)	–S11	2.669(7)
<Ag10–S>	**2.534**	**<Ag11–S>**	**2.525**	**<Ag12–S>**	**2.526**

TABLE 4 (*contd.*)

$[Ag_{10}(Hg,Cu)As_2S_8]^{2+}$ *B layer*					
As5–S16	2.306(5)	As6–S22	2.159(8)		
–S21	2.261(5)	–S24	2.188(5)		
–S26	2.295(7)	–S25	2.256(5)		
<As5–S>	**2.287**	**<As6–S>**	**2.201**		
As7–S17	2.253(8)	As8–S28	2.242(6)		
–S23	2.229(5)	–S27	2.319(5)		
–S29	2.249(5)	–S30	2.348(8)		
<As7–S>	**2.244**	**<As8–S>**	**2.303**		
Hg1/Cu1–S19	2.323(6)	Hg2/Cu2–S18	2.348(6)		
–S20	2.386(6)	–S31	2.321(5)		
<Hg1/Cu1–S>	**2.355**	**<Hg2/Cu2–S>**	**2.335**		
Ag20–S18	2.355(6)	Ag29–S28	2.510(6)	Ag32–S29	2.321(7)
–S18	2.355(6)	–S21	2.539(6)	–S29	2.321(7)
<Ag20–S>	**2.355**	**<Ag29–S>**	**2.525**	**<Ag32–S>**	**2.321**
Ag34–S25	2.433(6)	Ag33–S22	2.473(6)	Ag13–S23	2.429(7)
–S25	2.433(6)	–S31	2.626(7)	–S6	2.528(5)
<Ag34–S>	**2.433**	–S24	2.625(5)	–S30	2.591(5)
		<Ag33–S>	**2.575**	**<Ag13–S>**	**2.516**
Ag14–S9	2.434(6)	Ag15–S1	2.452(6)	Ag21 –S13	2.529(6)
–S21	2.593(7)	–S25	2.630(5)	–S26	2.763(5)
–S22	2.667(5)	–S23	2.694(5)	–S29	2.795(7)
<Ag14–S>	2.565	–S18	2.862(7)	–S20	2.787(5)
		<Ag15–S>	**2.660**	**<Ag21–S>**	**2.719**
Ag22–S26	2.397(6)	Ag26–S11	2.516(7)	Ag28–S17	2.561(5)
–S27	2.508(5)	–S21	2.521(5)	–S8	2.550(6)
–S19	2.916(7)	–S27	2.588(5)	–S16	2.723(8)
<Ag22–S>	**2.607**	–S20	2.898(8)	–S18	2.956(5)
		<Ag26–S>	**2.631**	**<Ag28–S>**	**2.698**
Ag16–S5	2.448(7)	Ag17–S7	2.425(6)	Ag18–S3	2.505(7)
–S24	2.588(5)	–S26	2.498(5)	–S28	2.525(5)
–S29	2.622(5)	–S24	2.600(7)	–S16	2.563(5)
–S19	2.852(7)	–S31	2.919(5)	–S31	2.899(8)
<Ag16–S>	**2.628**	**<Ag17–S>**	**2.611**	**<Ag18–S>**	**2.623**
Ag19–S2	2.426(6)	Ag23–S4	2.526(6)	Ag24–S22	2.589(5)
–S28	2.543(7)	–S30	2.582(5)	–S10	2.584(6)
–S17	2.706(5)	–S31	2.601(5)	–S27	2.692(7)
–S19	2.750 (5)	–S25	2.764(7)	–S19	2.767(5)
<Ag19–S>	**2.606**	**<Ag23–S>**	**2.618**	**<Ag24–S>**	**2.658**
Ag25–S16	2.442(5)	Ag27–S17	2.484(6)	Ag30 –S19	2.497(6)
–S30	2.528(6)	–S23	2.514(5)	–S19	2.497(6)
–S18	2.671(7)	–S20	2.778(7)	–S24	2.740(6)
–S20	2.764(5)	–S18	2.762(5)	–S24	2.740(6)
<Ag25–S>	**2.601**	**<Ag27–S>**	**2.635**	**<Ag30–S>**	**2.619**
Ag31–S20	2.353(6)				
–S31	2.532(6)				
–S16	2.790(7)				
–S27	2.875(6)				
<Ag31–S>	**2.638**				

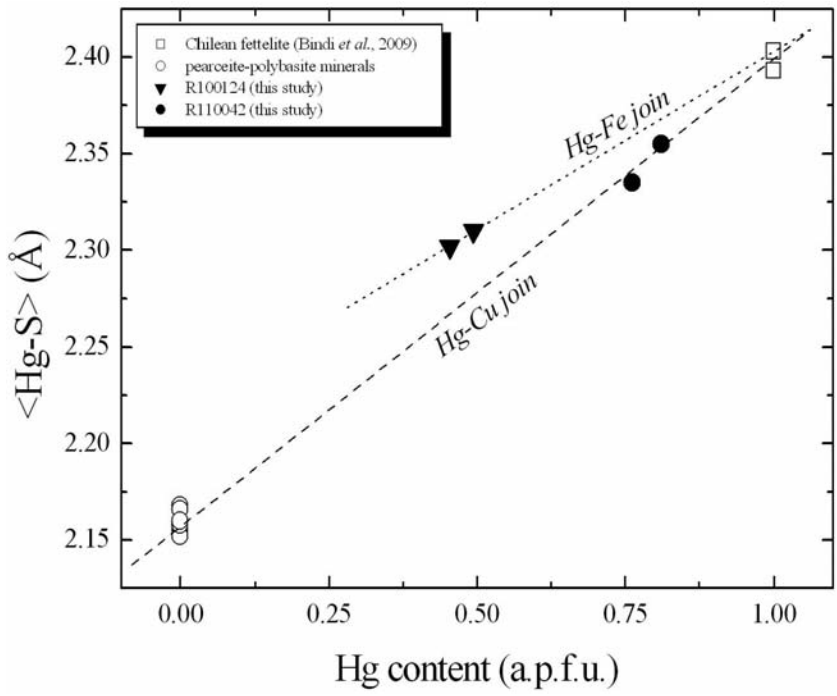

FIG. 4. The relationship between the Hg content (a.p.f.u.) and the <Hg–S> distance (Å) for fettelite samples and for different members of the pearceite–polybasite group (see text). The dashed and dotted lines indicate the possible Hg–Cu and Hg–Fe joins for fettelite.

only requirement of a new fettelite-like mineral. As Cu is usually monovalent in these minerals [as confirmed by the excellent regression line shown in Fig. 4 (R = 0.996) which uses the Cu–S distances in pearceite–polybasite, where Cu is in a monovalent state], the $Cu^{+} \leftrightarrow Hg^{2+}$ substitution would produce an excess negative charge. To maintain charge balance in a Cu-dominant mineral, another coupled substitution must occur, such as the replacement of Ag by a divalent cation (e.g. Zn, Pb). This type of replacement could occur either by random substitutions for Ag in the 34 available structural positions (i.e. in a disordered fashion) or in a more ordered manner at certain selected positions. For R110042, despite the high-quality structural data, we were not able to locate (in the refinements of the occupancy factors of the 34 Ag positions) a divalent lighter and/or heavier cation substituting for Ag. This might indicate that the divalent cation balancing the entry of copper substituting for mercury was distributed randomly among the available Ag positions.

Metal–metal bonding

Metal–metal bonding is a mechanism that may have an effect on the chemical variability at the Hg sites without the need to invoke charge-balance considerations. For instance, in pyrite, charge balance constraints are removed by S–S bond interactions, and a similar role is played by Ni–Ni bonds in heazlewoodite (Gibbs *et al.*, 2005, 2008). As a number of the Ag–Ag distances in fettelite are similar to those observed in face-centred cubic silver [$r_{(Ag-Ag)}$ = 2.89 Å; Suh *et al.*, 1988] or hexagonal close-packed silver [$r_{(Ag-Ag)}$ = 2.93 Å; Petruk *et al.*, 1970], an investigation of the possibility of metal–metal bonding in fettelite following the Bader model (Bader, 1990) seemed worthwhile. In this model, a pair of atoms is considered to exhibit a bond interaction if the electron density distribution indicates that a minimum energy bond path joins them, and if the pair of atoms shares a zero-flux interatomic surface. Therefore, using *SPEEDEN* software (Downs *et al.*, 2002), the procrystal electron density distribution for sample R100124 was calculated and bond paths were determined.

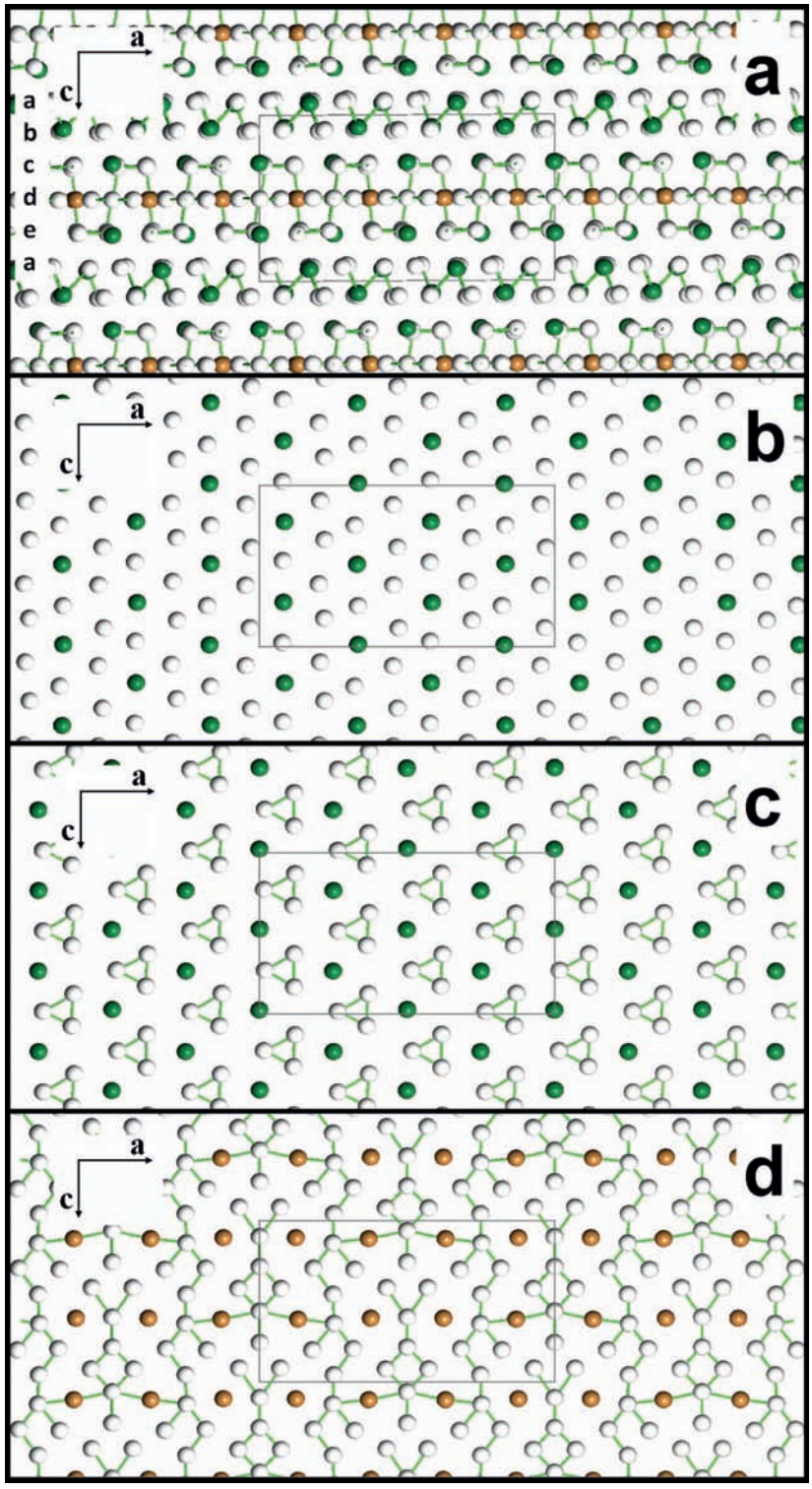
a
c
a
b
c
d
e
a
a
c
b
a
c
c
a
c
d

Figure 5*a* shows the fettelite metal atoms, without S, looking along the *b* axis, in a similar orientation to that shown in Fig. 3. Five distinct layers are observed, with a–b corresponding to module layer *A* in Fig. 3, and c–d–e corresponding to module layer *B*. The green lines joining pairs of metal atoms indicate bonds. Layer d has a composition $(Fe,Hg)Ag_4$, whereas the other layers are all $AsAg_3$, with layers a = b and c = e. There are As–Ag bonds between layers a and b, with $\langle r_{(As-Ag)} \rangle$ = 3.30 Å, and a range from 3.17 to 3.49 Å, but no bond interactions within the layer, as shown in Fig. 5*b*. The layers a and b represent well-ordered close-packed monolayers with relatively little distortion. In contrast, layers c and e have the same composition as layers a and b, but are much more distorted due to the presence of bonded clusters containing three Ag atoms, as indicated in Fig. 5*c*. The mean $\langle r_{(Ag-Ag)} \rangle$ is 3.04 Å, with a range from 2.88 to 3.24 Å. Layer d is composed only of Ag and (Fe,Hg) atoms. The Ag–Ag average $\langle r_{(Ag-Ag)} \rangle$ = 2.92 Å, with a range from 2.74 to 3.29 Å. The short Ag–Ag distances indicate that this layer has the strongest Ag–Ag bond interactions. The (Fe,Hg) is only bonded to Ag atoms within this layer, with $r_{(Ag-(Fe,Hg))}$ values ranging from 3.19 to 3.47 Å, as shown in Fig. 5*d*. The metal atoms in layers c–d–e have (Fe,Hg)–Ag bond distances of 2.98 and 3.10 Å, and three Ag–Ag bonds ranging from 3.05 to 3.12 Å in length.

Metal–metal interactions can affect both charge balance and the conductivity of the crystal (Gibbs *et al.*, 2005). In this context, there is a continuous two-dimensional network of bond interactions in module layer *B*, as demonstrated in Fig. 5, which is not present in module layer *A*, or along the *c* axis. As such, fettelite crystals might be expected to have significantly anisotropic electrical conductivities, with a greater conductivity in the a–b plane. As the continuous bond network in layer d is broken up by larger gaps around the (Fe,Hg) site, chemical variably in this site could produce a variable conductivity in the a–b plane. This feature is in perfect agreement with that observed by Bindi and Menchetti (2011) for HT-fettelite. In this HT-structure, the disorder responsible for the ionic conductivity is located in the *B* layer where the Ag–Hg cations are found in various sites corresponding to the most pronounced probability density function locations of diffusion-like paths.

Concluding remarks

On the basis of structural information gained from the characterization of fettelite from the type locality (including the holotype specimen), we can confirm that the crystal-chemical formula originally reported by Wang and Paniagua (1996) should be revised to $[Ag_6As_2S_7][Ag_{10}HgAs_2S_8]$ (Z = 8). The refined compositions of the crystals in this study, $[Ag_6As_2S_7][Ag_{10}(Fe_{0.53}Hg_{0.47})As_2S_8]$ (R100124) and $[Ag_6As_2S_7][Ag_{10}(Hg_{0.79}Cu_{0.21})As_2S_8]$ (R110042), clearly indicate that new minerals related to fettelite exist. Indeed, it seems likely that a new fettelite-like mineral, which has Fe dominant over Hg in two structural positions, occurs at the type locality. A new fettelite-like mineral with Cu substituting for Hg and, for charge balance requirements, a divalent cation randomly substituting for Ag (in a disordered fashion) may also occur. It is not surprising to see such differences in chemistry for crystals coming from the same occurrence (Odenwald, Germany). Minerals belonging to the pearceite–polybasite group, for example, which are strongly related to fettelite, exhibit similar chemical variability.

FIG. 5 (*facing page*). The structure of R100124 fettelite with metal atoms displayed as spheres, and S atoms not shown. White, green and brown spheres correspond to Ag, As, and (Fe,Hg), respectively. The green lines indicate metal–metal bond interactions as determined by a procrystal electron density analysis. The figure is in the same orientation as Fig. 3, viewed along the *b* axis. (*a*) The module layer *A* is composed of 2 metal layers, a–b, and module layer *B* is composed of metal layers c–d–e. (*b*) A representation of the metal atoms in layers a (or equivalently b). Although the Ag and As atoms form a relatively undistorted close-packed monolayer, there is no metal–metal bonding in the layer, only between layers a–b. (*c*) A representation of the metal atoms in layers c (or equivalently e), showing a more distorted monolayer than layer a or b, with bonded clusters containing three Ag atoms. (*d*) A representation of the metal atoms in layer d showing a continuous network of Ag–Ag and Ag–(Fe,Hg) bonds, suggesting a strongly metallic character that probably produces a significantly greater electrical conductivity in the plane of the layer than that in the *c* direction. The distortion around the (Fe,Hg) sites suggests that chemical substitutions could produce tuneable electrical properties.

Acknowledgements

This work was funded by the CNR (Istituto di Geoscienze e Georisorse, sezione di Firenze) and by the M.I.U.R., P.R.I.N. 2009 project "Modularity, microstructures and non-stoichiometry in minerals" issued to Paola Bonazzi, and by Newmont Mining Co for RTD to study copper and silver sulfide minerals. The holotype material from the University of Heidelberg was kindly provided by Rainer Altherr. The manuscript was improved by comments of Frantisek Laufek and one anonymous reviewer.

References

Bader, R.F.W. (1990) *Atoms in Molecules*. Oxford Science Publications, Oxford, UK.

Bindi, L. and Menchetti, S. (2011) Fast ion conduction character and ionic phase-transition in silver sulfosalts: the case of fettelite $[Ag_6As_2S_7][Ag_{10}HgAs_2S_8]$. *American Mineralogist*, **96**, 792–796.

Bindi, L., Evain, M. and Menchetti, S. (2006) Temperature dependence of the silver distribution in the crystal structure of natural pearceite, $(Ag,Cu)_{16}(As,Sb)_2S_{11}$. *Acta Crystallographica*, **B62**, 212–219.

Bindi, L., Evain, M., Spry, P.G. and Menchetti, S. (2007*a*) The pearceite–polybasite group of minerals: crystal chemistry and new nomenclature rules. *American Mineralogist*, **92**, 918–925.

Bindi, L., Evain, M. and Menchetti, S. (2007*b*) Complex twinning, polytypism and disorder phenomena in the crystal structures of antimonpearceite and arsenpolybasite. *The Canadian Mineralogist*, **45**, 321–333.

Bindi, L., Evain, M., Spry, P.G., Tait, K.T. and Menchetti, S. (2007*c*) Structural role of copper in the minerals of the pearceite–polybasite group: the case of the new minerals cupropearceite and cupropolybasite. *Mineralogical Magazine*, **71**, 641–650.

Bindi, L., Keutsch, F.N., Francis, C.A. and Menchetti, S. (2009) Fettelite, $[Ag_6As_2S_7][Ag_{10}HgAs_2S_8]$ from Chañarcillo, Chile: crystal structure, pseudosymmetry, twinning, and revised chemical formula. *American Mineralogist*, **94**, 609–615.

Downs, R.T., Gibbs, G.V., Boisen, M.B. Jr and Rosso, K.M. (2002) A comparison of procrystal and *ab initio* representations of the electron-density distributions of minerals. *Physics and Chemistry of Minerals*, **29**, 369–385.

Evain, M., Bindi, L. and Menchetti, S. (2006) Structural complexity in minerals: twinning, polytypism and disorder in the crystal structure of polybasite, $(Ag,Cu)_{16}(Sb,As)_2S_{11}$. *Acta Crystallographica*, **B62**, 447–456.

Gibbs, G.V., Downs, R.T., Prewitt, C.T., Rosso, K.M., Ross, N.L. and Cox, D.F. (2005) Electron density distributions calculated for the nickel sulfides millerite, vaesite and heazlewoodite and nickel metal: a case for the importance of Ni–Ni bond paths for electron transport. *Journal of Physical Chemistry B*, **109**, 21788–21795.

Gibbs, G.V., Downs, R.T., Cox, D.F., Ross, N.L., Prewitt, C.T., Rosso, K.M., Lippmann, T. and Kirfel, A. (2008) Bonded interactions and the crystal chemistry of minerals: a review. *Zeitschrift fur Kristallographie*, **223**, 1–40.

Nespolo, M. (2004) Twin point groups and the polychromatic symmetry of twins. *Zeitschrift für Kristallographie*, **219**, 57–71.

Oxford Diffraction (2006) *CrysAlis RED (Version 1.171.31.2) and ABSPACK in CrysAlis RED*. Oxford Diffraction Ltd, Abingdon, Oxfordshire, England.

Petříček, V., Dušek, M. and Palatinus, L. (2006) *JANA2000, a crystallographic computing system*. Institute of Physics, Academy of Sciences of the Czech Republic, Prague, Czech Republic.

Petruk, W., Cabri, L.J., Harris, D.C., Stewart, J.M. and Clark, L.A. (1970) Allargentum, redefined. *The Canadian Mineralogist*, **10**, 163–172.

Suh, I.-K., Ohta, H. and Waseda, Y. (1988) High-temperature thermal expansion of six metallic elements measured by dilatation method and X-ray diffraction. *Journal of Materials Science*, **23**, 757–760.

Wang, N. and Paniagua, A. (1996) Fettelite, a new Hg-sulfosalt mineral from Odenwald. *Neues Jahrbuch für Mineralogie Monatshefte*, **1996**, 313–320.